

SUPPORTING INFORMATION

Conformational Modulation of the Farnesoid X Receptor

by Prenylflavonoids: Insights from Hydrogen Deuterium Exchange Mass Spectrometry (HDX-MS), Fluorescence Titration and Molecular Docking Studies

Liping Yang¹, David Broderick¹, Yan Campbell^{4,6}, Adrian F. Gombart^{4,6}, Jan F. Stevens^{4,5},
Yuan Jiang³, Victor L. Hsu^{6*}, William H. Bisson^{2*}, and Claudia S. Maier^{1,4*}

¹ Department of Chemistry, Oregon State University, Corvallis, OR 97331

² Department of Environmental and Molecular Toxicology, Oregon State University,
Corvallis, OR 97331

³ Department of Statistics, Oregon State University, Corvallis, OR 97331

⁴ Linus Pauling Institute, Oregon State University, Corvallis, OR 97331

⁵ Department of Pharmaceutical Sciences, Oregon State University, Corvallis, OR 97331

⁶ Department of Biochemistry and Biophysics, Oregon State University, Corvallis, OR 97331

Corresponding authors:

Victor L. Hsu

hsuv@science.oregonstate.edu

+1-541-737-4398

William H. Bisson

bissonw@science.oregonstate.edu

+1-541-737-5735

Claudia S. Maier

claudia.maier@oregonstate.edu

+1-541-737-9533

Figure S1: (A) Global HDX uptake plots of FXR-LBD with/without DMSO (3.3% v/v); (B) Fluorescence emission spectra of FXR-LBD with/without DMSO (3.3% v/v).

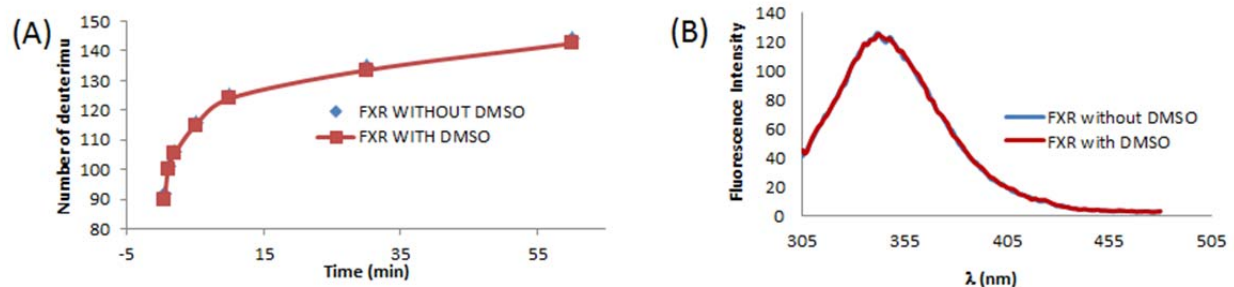
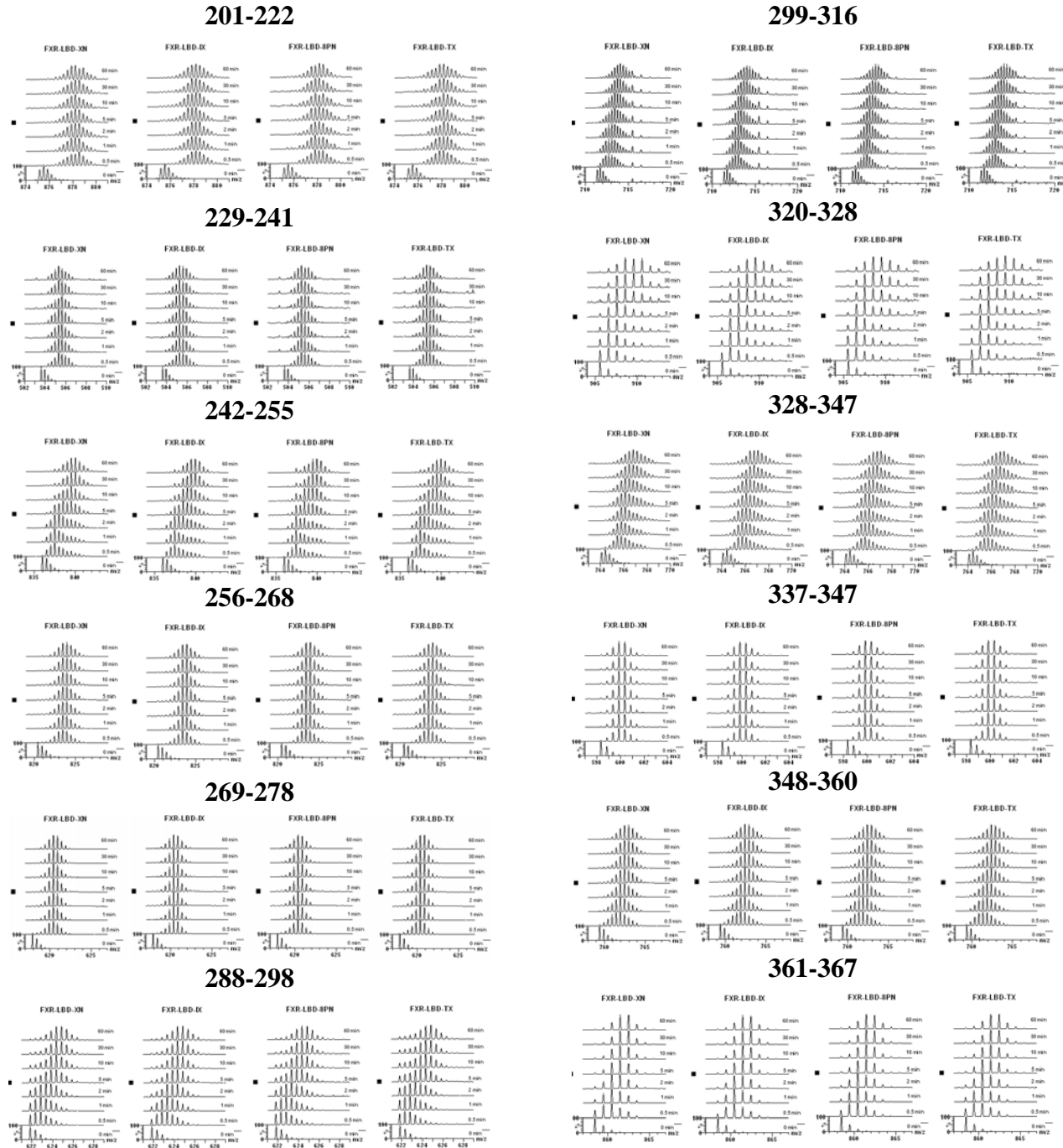
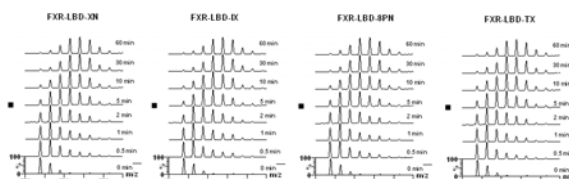


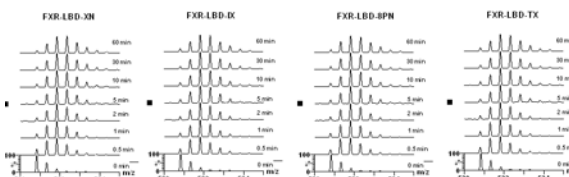
Figure S2: High resolution accurate mass spectra of peptic peptide demonstrating evolution of deuterium incorporation as a function of time. The partial sequence of each peptide is depicted at the top of each panel. Deuteration times (0, 0.5, 1, 2, 5, 10, 30, 60 min) are denoted in each panel.



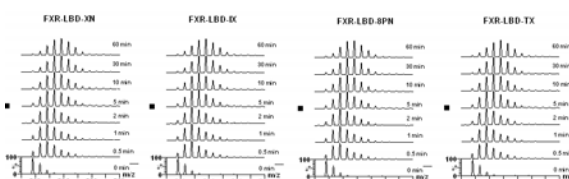
368-375



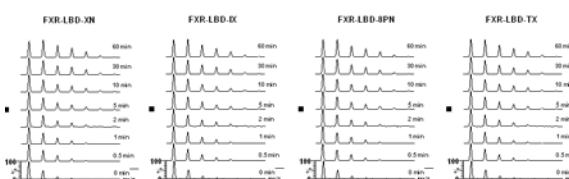
388-396



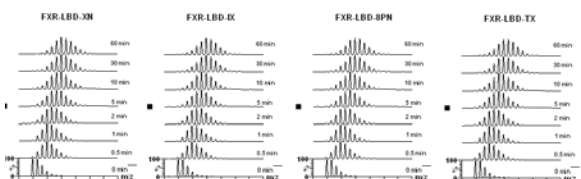
397-405



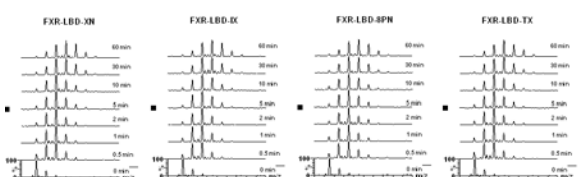
406-412



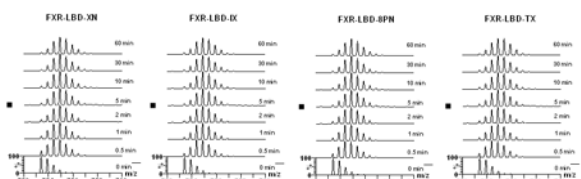
419-433



434-440



440-451



454-465

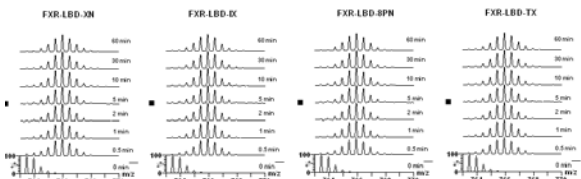


Figure S3: Global HDX uptake plots for the apo FXR-LBD in comparison to the FXR-LBD in presence of ligands. For each ligand tested HDX-MS analysis was conducted in triplicate, and the error bars represent the standard deviation.

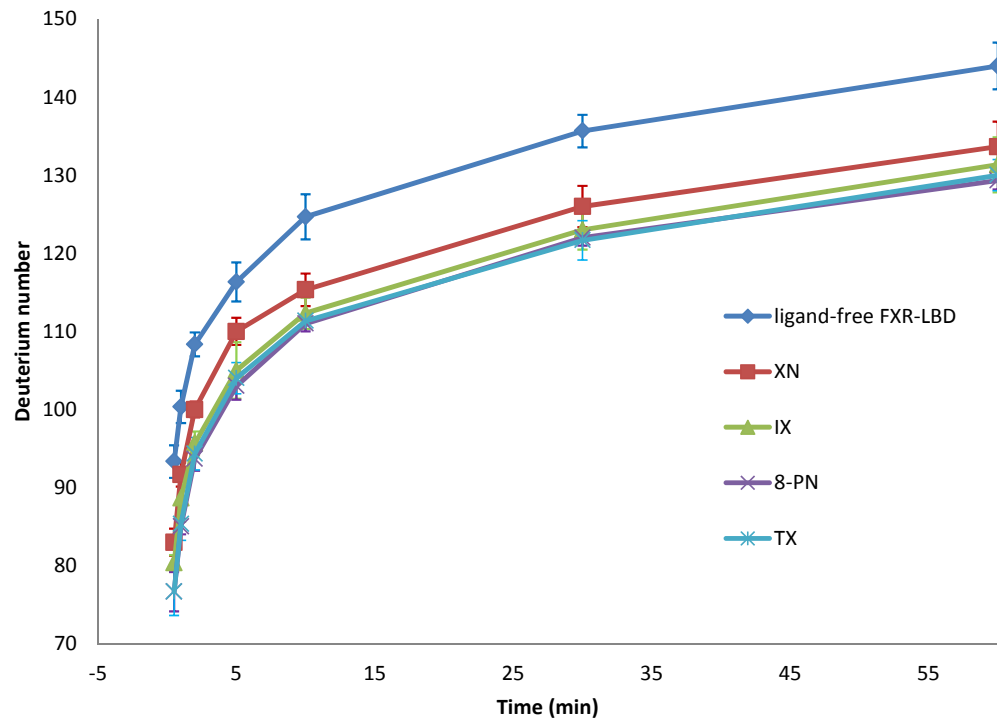
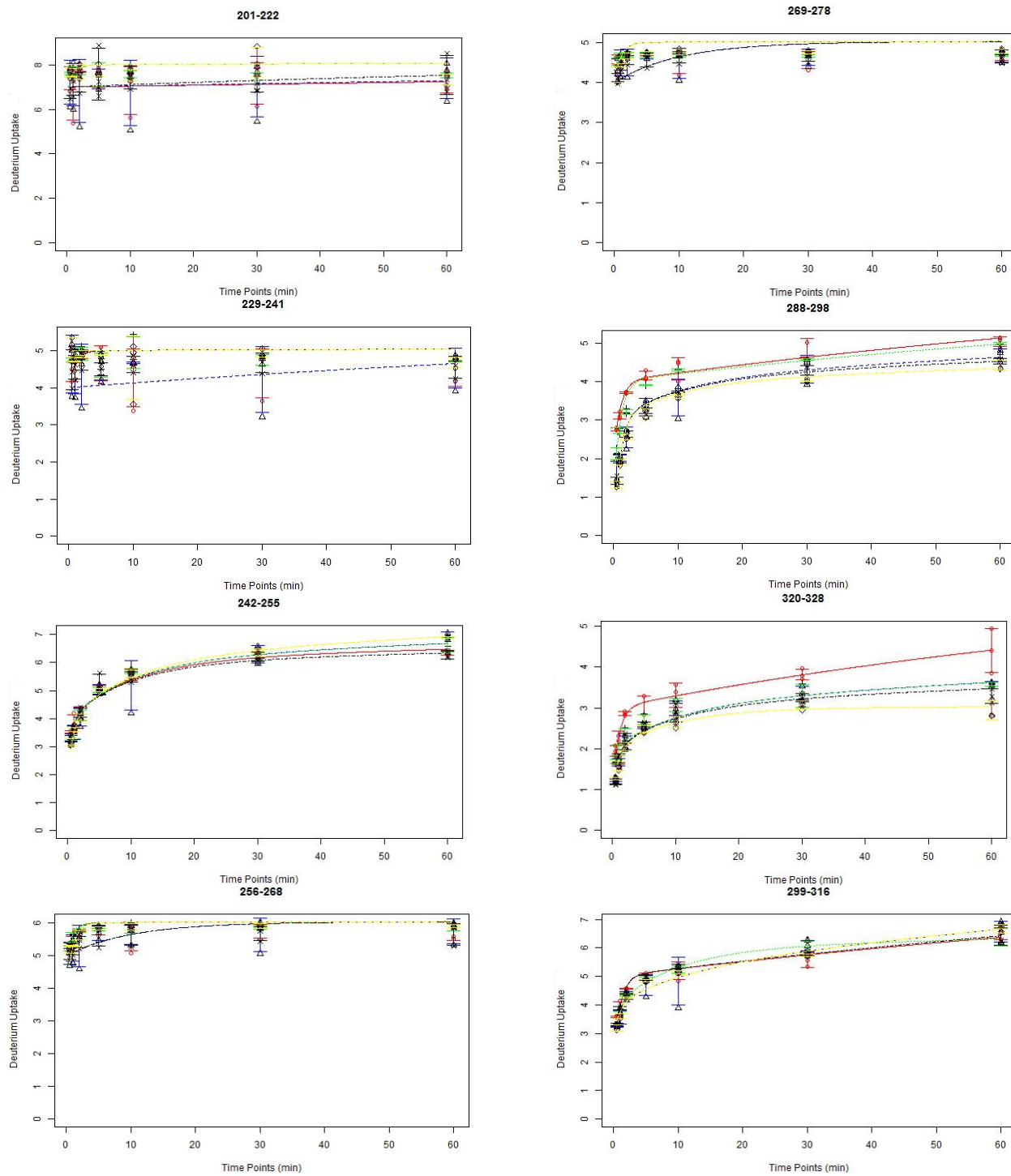
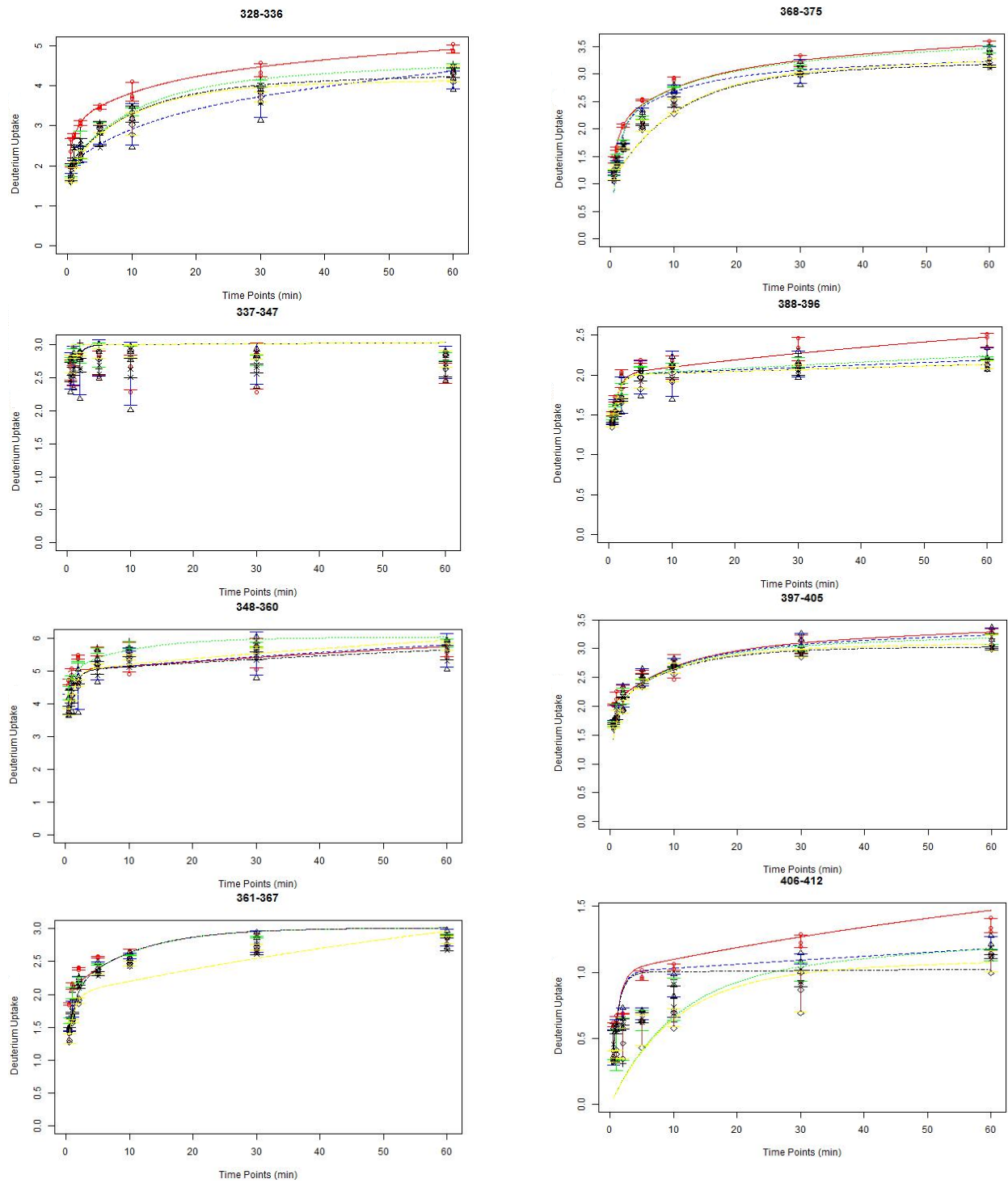


Figure S4: Deuterium incorporation level for each peptide at seven exchange-in time points (0.5, 1, 2, 5, 10, 30, 60 min). Each data point shows the error bar based on the three experimental replicates. Color code: apo-FXR-LBD, red; XN, blue; IX, green; 8-PN, black; TX, yellow.





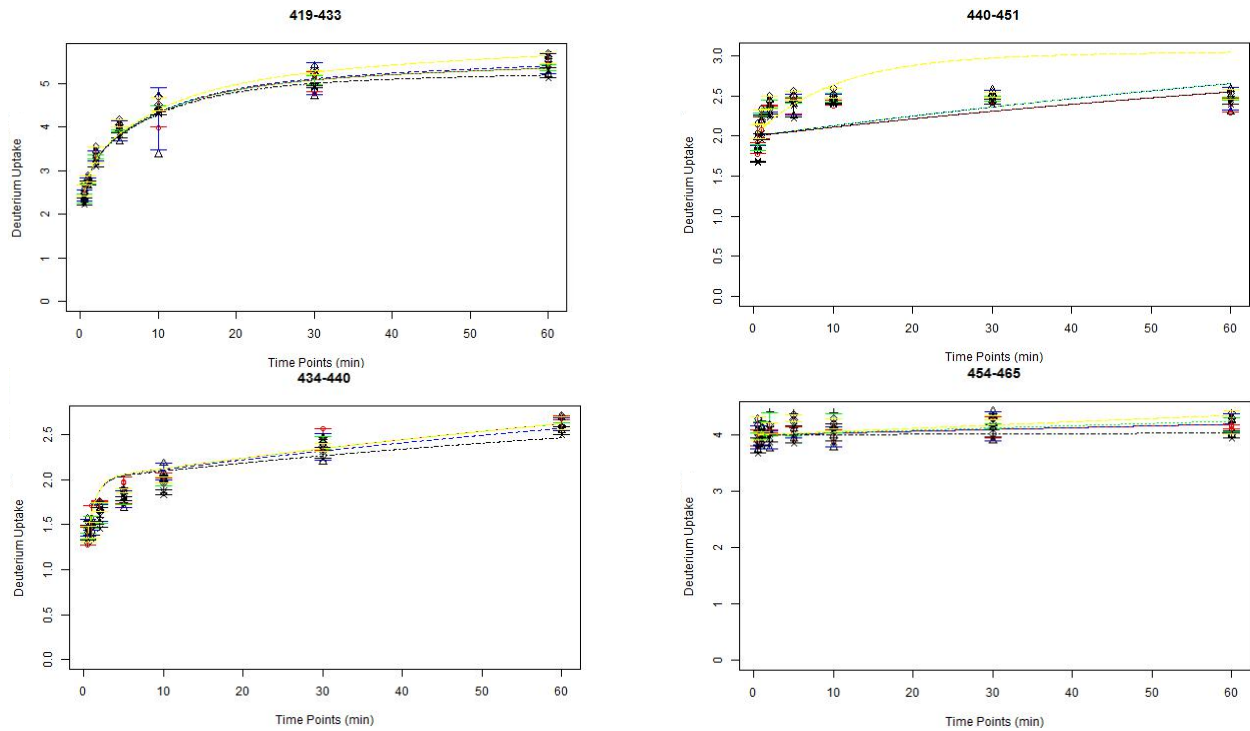


Figure S5: Peptide-level HDX profiles of FXR-LBD in presence of prenylflavonoids. Deuterium exchange-in percentage is shown at different labeling time points (0.5, 1, 2, 5, 10, 30, and 60 min, from left to right) for each peptide. Asterisks mark peptides encompassing residues which have no secondary structure assigned in the crystal structure of 3-deoxy-CDCA bound FXR-LBD- (PDB 1OT7).

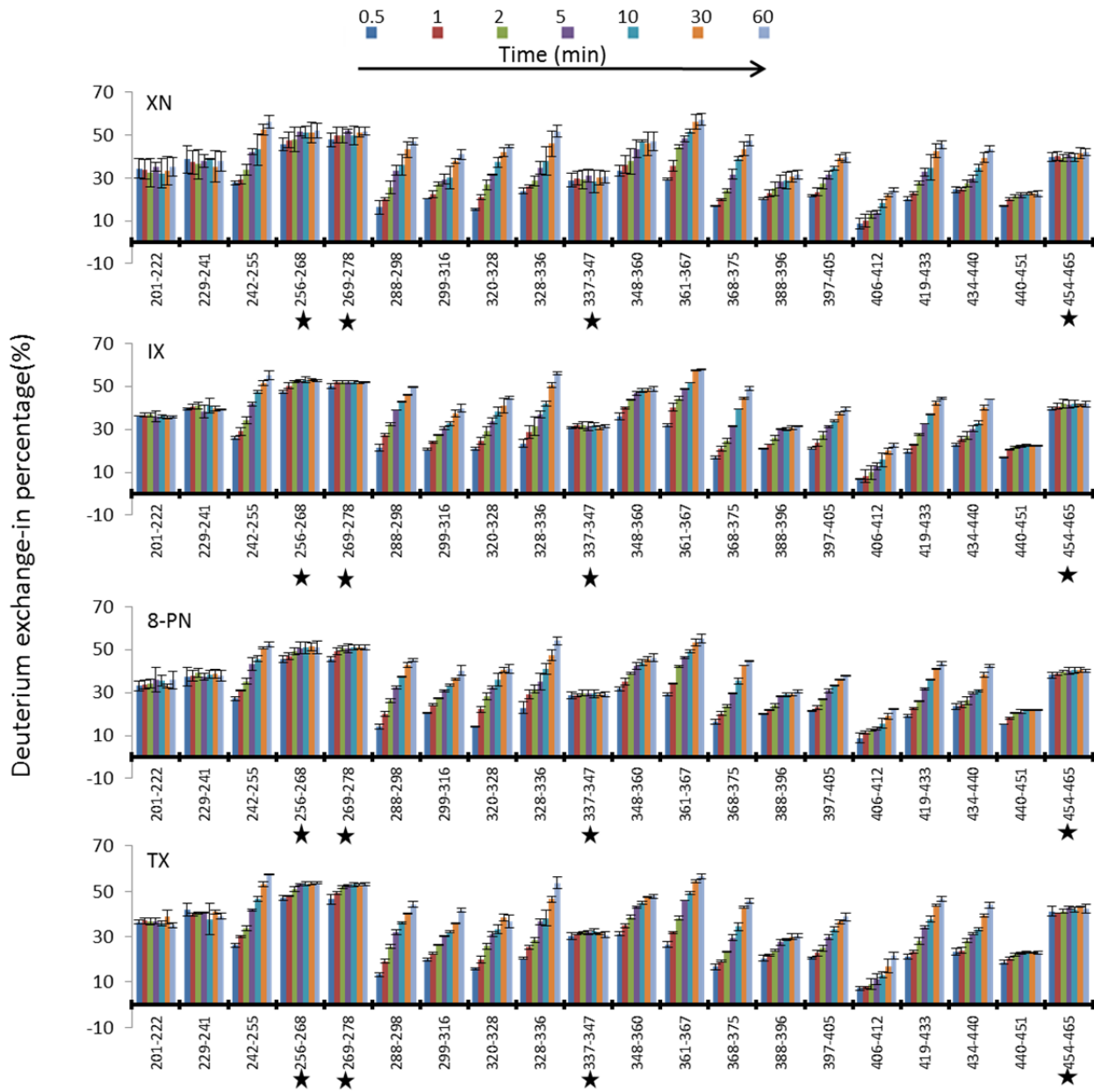


Figure S6: Mass spectrometric detection of the modification of the FXR-LBD by XN.

- (A) The proposed Michael addition reaction between the α,β -unsaturated ketone functionality in XN and a cysteine thiol group in the FXR-LBD.
- (B) LC-MS spectra of FXR-LBD ($\sim 10\mu\text{M}$) in presence of XN ($\sim 180\mu\text{M}$) as a function of reaction time. The mass spectra demonstrate that the current construct of FXR-LBD can be covalently modified *in vitro* by multiple XN molecules (in agreement with that the construct has 6 cysteine residues [Yang et al. *Biochim Biophys Acta*. **2014**, 1844, 1684-93]).

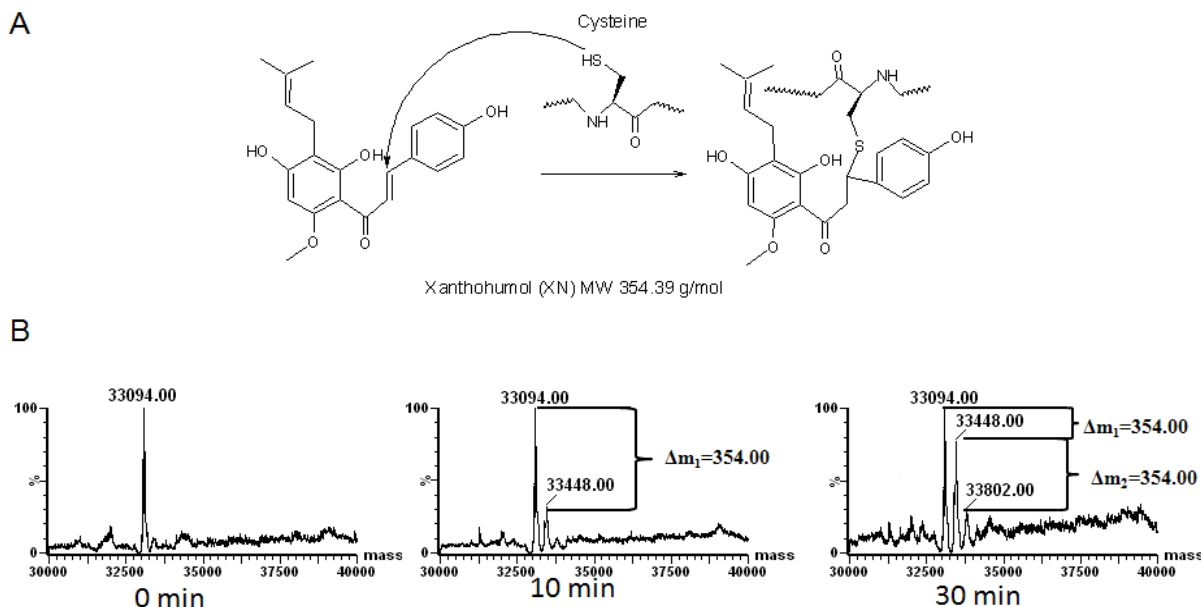


Table S1. Average differences in deuterium incorporation levels for each of the peptides used in the current HDX-MS study.

The values were obtained by averaging the differences in deuterium levels across the seven reaction time points (0.5, 1, 2, 5, 10, 30 to 60 min) used in the current time course study. A negative percentage indicates the increase of protection against deuterium exchange-in upon ligand binding and a positive number indicates less protection in a particular region of the FXR-LBD ligand complex. Deuterium level differences of regions with $p = <0.001$, calculated by two-way ANOVA, are considered as statistically significant.

Residue ^a	Charge ^b	apo ^c	XN-apo ^d	P-value	IX-apo ^e	P-value	8PN-apo ^f	P-value	TX-apo ^g	P-value
201-222	3	34%	-1%	0.707	2%	0.028	0%	0.845	2%	0.012
229-241	2	38%	0%	0.945	2%	0.017	1%	0.523	3%	0.025
242-255	2	42%	-1%	0.210	-1%	0.048	-1%	0.058	0%	0.208
256-268	2	51%	-1%	0.263	1%	0.078	-1%	0.075	1%	0.233
269-278	2	51%	-1%	0.459	1%	0.037	-1%	0.045	0%	0.397
288-298	2	40%	-8%	<0.001	-3%	<0.001	-9%	<0.001	-10%	<0.001
299-316	3	31%	-1%	0.108	0%	0.306	0%	0.467	-1%	0.003
320-328	1	38%	-7%	<0.001	-5%	<0.001	-7%	<0.001	-9%	<0.001
328-336	2	44%	-9%	<0.001	-6%	<0.001	-7%	<0.001	-9%	<0.001
337-347	2	29%	0%	0.768	2%	0.002	0%	0.833	2%	0.013
348-360	2	44%	-1%	0.017	0%	0.452	-4%	<0.001	-3%	<0.001
361-367	1	49%	-3%	<0.001	-2%	<0.001	-5%	<0.001	-6%	<0.001
368-375	2	35%	-3%	<0.001	-3%	<0.001	-5%	<0.001	-5%	<0.001
388-396	2	29%	-2%	<0.001	-1%	0.005	-3%	<0.001	-3%	<0.001
397-405	2	32%	-1%	0.005	-2%	<0.001	-2%	<0.001	-3%	<0.001
406-412	1	19%	-3%	<0.001	-5%	<0.001	-4%	<0.001	-6%	<0.001
419-433	3	32%	0%	0.711	0%	0.326	-1%	0.028	1%	0.014
434-440	1	33%	-1%	0.083	-1%	0.021	-2%	0.011	-1%	0.028
440-451	2	21%	0%	0.111	1%	0.004	-1%	0.004	1%	0.002
454-465	2	40%	0%	0.909	1%	0.030	-1%	0.033	1%	0.004

- a) Residue numbers for the full-length FXR-LBD (UniRef100_B6ZGS9)
- b) Charge state of each peptide observed in the LC-MS experiment.
- c) Deuterium level of each peptide in apo FXR-LBD.
- d) Deuterium level difference percentage between XN and apo FXR-LBD.
- e) Deuterium level difference percentage between IX and apo FXR-LBD.
- f) Deuterium level difference percentage between 8-PN and apo FXR-LBD.
- g) Deuterium level difference percentage between TX and apo FXR-LBD.

Table S2. Amide hydrogen distribution for each peptide derived by applying a six-fixed-rate-constant binning model to fit the deuterium uptake plots. Exchange rate bins were grouped into three categories: fast (10^1 and 10^0 min^{-1}), medium (10^{-1} and 10^{-2} min^{-1}), and slow (10^{-3} and 10^{-4} min^{-1}) for the discussion of the data.

from to	backbo ne	apo-FXR-LBD					XN					IX					8-PN					TX										
		10^1	10^0	10^{-1}	10^{-2}	10^{-3}	10^{-4}	10^1	10^0	10^{-1}	10^{-2}	10^{-3}	10^{-4}	10^1	10^0	10^{-1}	10^{-2}	10^{-3}	10^{-4}	10^1	10^0	10^{-1}	10^{-2}	10^{-3}	10^{-4}							
201 222	21	7	0	0	1	0	13	7	0	0	0	4	10	7	1	0	0	0	13	7	0	0	1	0	13	7	1	0	0	0	13	
229 241	12	4	1	0	0	0	7	4	0	0	1	3	4	5	0	0	0	0	7	4	1	0	0	0	0	7	5	0	0	0	0	7
242 255	12	3	1	2	1	0	5	3	1	2	1	4	1	2	2	2	1	4	1	3	1	2	0	6	0	2	2	2	2	0	4	
256 268	11	5	1	0	0	0	5	5	0	1	0	0	5	5	1	0	0	0	5	5	0	1	0	0	5	4	2	0	0	0	5	
269 278	9	4	1	0	0	0	4	4	0	1	0	0	4	4	1	0	0	0	4	4	0	1	0	0	4	4	1	0	0	0	4	
288 298	10	2	2	0	2	4	0	0	3	1	1	3	2	1	3	0	2	1	3	0	3	1	1	1	4	0	3	1	0	6	0	
299 316	16	2	3	0	2	8	1	3	1	1	3	5	3	3	1	2	0	5	5	2	3	0	2	9	0	3	1	1	3	5	3	
320 328	8	1	2	0	4	0	1	1	1	1	1	3	1	2	0	1	1	3	1	1	1	1	1	0	4	1	1	1	0	0	5	
328 336	8	2	1	1	2	0	2	2	0	1	3	0	2	2	0	2	1	0	3	2	0	2	0	4	0	1	1	2	0	2	2	
337 347	9	2	1	0	0	0	6	2	1	0	0	0	6	3	0	0	0	0	6	2	1	0	0	0	6	3	0	0	0	0	6	
348 360	12	5	0	1	0	0	6	3	2	0	1	6	0	4	1	1	0	0	6	3	2	0	1	3	3	3	2	0	2	0	5	
361 367	5	2	0	1	0	0	2	1	1	1	0	0	2	1	1	1	0	0	2	1	1	1	0	0	2	1	1	0	2	1	0	
368 375	7	1	1	1	1	1	2	0	2	1	0	4	0	0	2	1	1	0	3	1	0	2	0	3	1	1	0	2	0	4	0	
388 396	7	1	1	0	1	0	4	1	1	0	0	3	2	1	1	0	0	4	1	1	1	0	0	2	3	1	1	0	0	2	3	
397 405	8	2	0	1	0	5	0	1	1	1	0	4	1	1	1	1	0	3	2	1	1	1	0	0	5	1	1	1	0	1	4	
406 412	5	0	1	0	1	0	3	0	1	0	0	3	1	0	0	1	0	3	1	0	1	0	0	0	4	0	0	1	0	1	3	
419 433	12	2	1	2	0	6	1	2	1	2	0	7	0	2	1	2	0	6	1	2	1	2	0	3	4	2	1	2	1	3	3	
434 440	6	1	1	0	1	3	0	1	1	0	1	2	1	1	1	0	1	3	0	1	1	0	1	0	3	1	1	0	1	3	0	
440 451	11	2	0	0	1	1	7	2	0	0	1	3	5	2	0	0	1	3	5	2	0	0	1	1	7	2	0	1	0	0	8	
454 465	10	4	0	0	0	3	3	4	0	0	0	3	3	4	0	0	0	4	2	4	0	0	0	0	6	4	0	0	0	6	0	

Table S3: ICM docking scores for the computational docking experiments of the ligands listed below into the ligand binding pocket of the human FXR-LBD (based on PDB 1OT7).

Ligand	Docking Score
3-Deoxy-CDCA	-26.63
XN	-22.38
TX	-22.03
IX	-11.73
8-PN	-10.83

Additional experimental details

Text S1: Fluorescence Quenching Data Analysis

For determining the ligand binding characteristics, quenching data were analyzed according to the Stern-Volmer equation,¹ which described the quenching process between a protein and a quencher:

$$\frac{F_0}{F} = 1 + K_{SV}[Q] \quad (1)$$

where F_0 and F are the fluorescence intensities in the absence and presence of the quencher (ligand), respectively; $[Q]$ is the concentration of the quencher. K_{SV} is the Stern-Volmer constant, which is related to the bimolecular quenching constant k_q , and τ_0 is the intrinsic fluorescence lifetime of the fluorophore in the absence of the quencher. K_{SV} is given by:

$$K_{SV} = k_q \tau_0 \quad (2)$$

A linear Stern-Volmer plot of $\frac{F_0}{F}$ versus $[Q]$ usually indicates that all the tryptophan residues in the protein are equally accessible to the quencher.

Non-linear Stern-Volmer plots with downward curvature concave towards the x-axis is an indication that only a fraction of the tryptophan residues are accessible to the quencher, and can be analyzed by using the Lehrer model,² i.e. the modified Stern-Volmer equation:

$$\frac{F_0}{F_0 - F} = \frac{1}{f_a [Q] K_{SV}} + \frac{1}{f_a} \quad (3)$$

where f_a is the fraction of the total tryptophan residues accessible to quencher.

Non-linear Stern-Volmer plots with upward curvature and concave towards the y-axis are characteristic of a combination of static and dynamic quenching, and can be analyzed by the following equation:¹

$$\frac{F_0}{F} = (1 + K_D[Q])(1 + K_S[Q]) \quad (4)$$

where K_D is the dynamic quenching constant and K_S is the static quenching constant.

For determination of dissociation constant K_d , binding data were analyzed by fitting the curve to the Hill equation:³

$$\frac{F_0 - F}{F_0} = \frac{[L]^n}{K_d + [L]^n} \quad (5)$$

All data fits, linear and non-linear regressions, were performed with the GraphPad Prism software and gave correlation coefficient (R) values exceeding 0.99.

- (1) Lakowicz, J. R., and SpringerLink (Online service). (2006) Principles of Fluorescence Spectroscopy, Third Edition. ed., Springer Science+Business Media, LLC, Boston, MA.
- (2) Lehrer, S. S. (1971) Solute perturbation of protein fluorescence. The quenching of the tryptophyl fluorescence of model compounds and of lysozyme by iodide ion, *Biochemistry* 10, 3254-3263.
- (3) Hill, A. V. (1913) The Combinations of Haemoglobin with Oxygen and with Carbon Monoxide. I, *Biochem. J.* 7, 471-480.

Text S2: Hierarchical clustering analysis of peptide-level HDX profiles

The main principle of hierarchical clustering is to iteratively identify two ligands (or ligand groups) with highest similarity for their local HDX profile by comparing their deuterium exchange-in level on each peptide, and cluster them into a ligand group, until all ligands are clustered into a single group. Initially, each ligand is assigned to its own cluster and then the algorithm proceeds iteratively, at each stage joining the two most similar clusters, continuing until there is just a single cluster. At each stage distances between clusters are recomputed using the complete linkage, i.e., the distance between those two elements (one in each cluster) that are farthest away from each other. A combination of a heat map with a dendrogram is used to illustrate the arrangement of the groups produced by hierarchical clustering.